Mon. Not. R. Astron. Soc. **000**, 000–000 (0000) Printed 25 October 1998 (MN LATEX style file v1.4)

Surface Imaging of Long-Period Variable Stars.

P.G. Tuthill,[1], C.A. Haniff[2] and J.E. Baldwin[2]
[1] *Space Sciences Laboratory, University of California at Berkeley, Berkeley, California 94720*
[2] *Astrophysics Group, Cavendish Laboratory, Madingley Road, Cambridge CB3 OHE*

Accepted 1998 December 99. Received 1998 November 99; in original form 1998 May 30

ABSTRACT
The photospheric surfaces of five long-period variables (o Ceti, R Leo, W Hya, χ Cyg, and R Cas) have been imaged in the optical/near-IR with the 4.2-m William Herschel Telescope. All exhibit departures from circular symmetry. Our data are consistent with the presence of bright compact features, individually contributing between 5 and 20 % of the total stellar flux, on each of the stars. The characteristics and behaviour of the features are similar to those reported on the surfaces of late-type supergiants, though the data presented here are inadequate to identify a common physical origin.

Key words: stars: – imaging – stars: individual: o Ceti – stars: individual: R Leo – stars: individual: W Hya – stars: individual: χ Cyg – stars: individual: R Cas – stars: long-period variables.

1 INTRODUCTION

The availability of high-resolution imaging methods now allows the detailed scrutiny of the surfaces of the nearest cool evolved stars. In the case of the prototypical M supergiant Betelgeuse (α Orionis), large departures from circular symmetry have been reported at radio (Lim et al. 1998), optical (Buscher et al. 1990), and ultraviolet (Gilliland & Dupre 1996) wavelengths, and recently Tuthill et al. (1997) have detected similar structures on α Her. and α Sco. For Mira-type variables, the evidence for similar departures from circular symmetry has also been accumulating, with workers generally choosing to interpret optical measurements in terms of limb-darkened disks with either elliptical distortions (Karovska et al. 1991; Wilson et al. 1992; Quirrenbach et al. 1992; Weigelt et al. 1996) or asymmetric bright features (Haniff, Scholz & Tuthill 1995; Bedding et al. 1994; Burns et al. 1998).

However, there is as yet no consensus as to the form of these distortions, and this lack of knowledge has hampered the elucidation of their physical origin: the presence of global elongations of the stellar photosphere would naturally suggest a quite different class of models than would bright asymmetric features.

Unfortunately, most previous speckle imaging studies of the nearest long-period variables have not allowed any detailed investigations of the morphologies of their surfaces. The failure of these studies can be traced to two principal sources: first, difficulties associated with the calibration of the speckle data, and second, problems related to the recovery of the Fourier phase information that allows for distinguishing between symmetric and non-centrosymmetric structures.

In this paper we present results from a multi-epoch program of optical interferometry of Mira variables using aperture masking methods at the 4.2 m William Herschel Telescope (WHT). This technique, which uses a mask in the telescope pupil to limit the range of spatial frequencies sampled, has been shown to improve both the calibration and phase recovery of speckle imaging experiments in the bright source limit (Haniff & Buscher 1992). Our new data thus provide a more detailed view of the stellar surfaces than has been achieved before.

Although a large number of stars were surveyed in total, we discuss here only the five largest (and hence most easily mapped) targets and restrict attention to the surface morphologies of this sample. Other aspects of the programme, for example the absolute sizes of the programme stars (o Ceti, R Leo, W Hya, χ Cyg, and R Cas) have been presented elsewhere (Tuthill et al. 1994a; Haniff, Scholz & Tuthill 1995; Tuthill et al. 1995). We include an appendix containing additional measurements of those programme stars that were only marginally resolved. These are not discussed in the main body of the paper, but our measurements may prove useful to other workers in the field.

2 OBSERVATIONS, DATA REDUCTION AND ANALYSIS

2.1 Observations

Observations were obtained at the Ground-Based High Resolution Imaging Laboratory of the 4.2 m WHT over six observing runs between January 1992 and September 1993. During each run a standard optical set-up using a collimat-

Table 1. Observing log. Calendar dates refer to the start of the night of each observation. The filter wavelengths and bandpasses (FWHM) are given in nm. The final three columns give the type of mask used, the effective aperture sizes in cm – diameter for holes, width for slits and the maximum baseline in m for the aperture mask corresponding to each observation.

Name	Date (m/y)	Stellar Phase	Mean JD -2.44×10^6	Filter $\lambda/\Delta\lambda$	Mask details Type	Ap. size	B_{max}
o Cet	01/92	0.58	8640	700/10	slit	10	4.2
	01/92	0.58	8640	710/10	slit	10	4.2
	07/92	0.05	8817	633/10	4-hole	31	3.5
	07/92	0.05	8817	700/10	5-hole	15	3.7
	07/92	0.05	8817	710/10	5-hole	15	3.7
	01/93	0.48	8991	700/10	slit	25?	3.8?
	09/93	0.22	9238	700/10	slit	31	3.8
	09/93	0.22	9239	710/10	slit	31	3.8
	12/93	0.49	9328	700/10	slit	113	3.7
	12/93	0.49	9328	710/10	slit	151	3.7
R Leo	01/92	0.27	8642	833/41	4-hole	30	3.8
	06/93	0.88	9149	700/10	slit	31	4.2
	06/93	0.88	9149	710/10	slit	31	4.2
W Hya	06/93	0.04	9147	700/10	slit	31	4.2
	06/93	0.04	9148	700/10	slit	31	4.2
	06/93	0.04	9148	710/10	slit	31	4.2
χ Cyg	07/92	0.32	8817	700/10	slit	31	3.8
	06/93	0.14	9148	633/10	slit	31	4.2
	06/93	0.14	9146	700/10	5-hole	16	3.8
	06/93	0.14	9147	710/10	slit	23	4.2
	09/93	0.35	9238	700/10	slit	62	3.8
R Cas	07/92	0.05	8817	700/10	slit	23	4.2
	07/92	0.05	8817	710/10	4-hole	31	3.5
	07/92	0.05	8817	710/10	slit	23	4.2
	06/93	0.82	9147	700/10	slit	31	4.2
	09/93	0.03	9238	700/10	slit	23	3.8
	09/93	0.03	9239	710/10	slit	31	3.8

ing lens, a pupil plane mask, and magnification optics was employed to convert the telescope into a multi-element interferometer. Images in the focal plane thus appeared as Airy disks crossed by sets of fringes, each set corresponding to a particular pair of transmitting apertures in the pupil mask. A variety of mask patterns were used, including four- and five-hole non-redundant designs, and in cases where the targets were particularly faint, a partially redundant narrow slit. Descriptions of the basic principles and implementation of the setup can be found in Buscher et al. (1990) and Wilson et al. (1992).

Data were obtained at a number of wavelengths, using interference filters centred at 633, 700, 710 and 833 nm with bandpasses (FWHM) of 10, 10, 10 and 41 nm respectively. Exposure times were between 7 and 10 ms, and approximately 20000 short-exposure interferograms were recorded per source. Identical observations of nearby unresolved calibration stars and close binaries were also secured to allow calibration of the transfer function of the apparatus and the focal plane scale and position angle. Errors in these were of order a few percent and 1 degree respectively.

Details of the observations, including the stars, dates, filters and observing geometry employed are given in Table 1.

2.2 Data reduction and analysis

Visibility amplitudes and closure phases, were extracted from the interferograms following standard methods (Haniff et al. 1987; Buscher et al. 1990), and were subsequently calibrated using the observations of the nearby point sources. In view of the fact that the targets were only marginally resolved, our quantitative analysis has been based on the fitting of simple models to the Fourier data rather than examining image reconstructions. These do, though, allow a qualitative presentation of the data (see, e.g. Figure 3).

As an example of our analysis we can consider R Cassiopeiae, whose monochromatic visibility curves are shown in Figure 1. Here, the decrease in normalised visibility with increasing baseline indicates that the star is resolved, with the more rapid drop at 710 nm implying that the star has a larger apparent size at this wavelength than at 833 nm and 700 nm. This type of figure, where information on the shape and size of the stellar brightness profile is presented either as a slice through the 2-dimensional visibility function or – as in this case – an azimuthally averaged visibility curve is that most commonly encountered in the literature.

However, plots such as those in Figure 1 shed little light on the deviations of the star from rotational symmetry. In order to assess any such deviations, we show the meas-

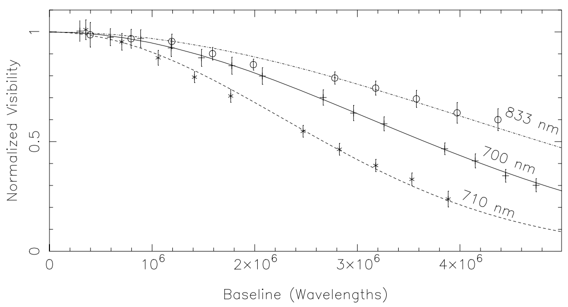

Figure 1. Azimuthally-averaged visibility functions for R Cassiopeiae from 1993 September. Date for three different filter bandpasses (700/10, 710/10 and 833/41 nm) are shown. The Gaussian FWHM of the inferred brightness profiles are 26.7, 34.4 and 20.3 mas respectively.

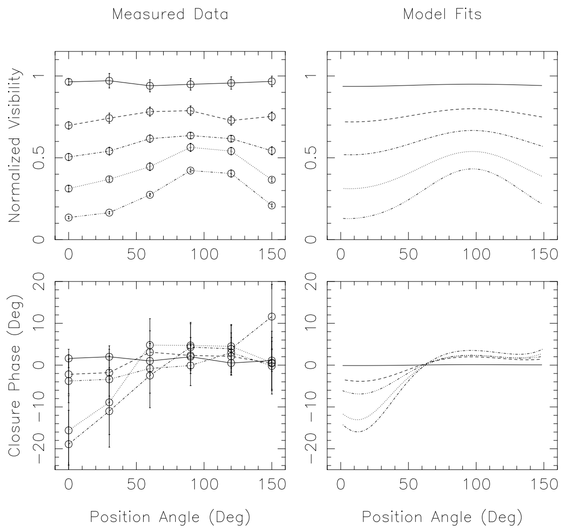

Figure 2. Calibrated visibility amplitudes and closure phases for R Cas at 710 nm as measured in 1992 July. The left-hand panels show the measured data, and the right-hand panels the predictions of a model composed of a circular disc together with two unresolved hotspots on the stellar surface. For clarity, only data corresponding to 5 of the interferometer baselines and 5 of the closure triangles are shown. In these, and subsequent plots, lower visibilities correspond to longer interferometer baselines. One-sigma error bars are plotted. For a centro-symmetric source all the closure phases should be zero.

ured Fourier amplitudes and closure phases for R Cas. in more detail in Figure 2. In the upper left panel the visibility amplitudes on five baselines of increasing length are plotted as a function of the orientation of the baseline on the sky. As expected for a resolved source, the mean visibility amplitude decreases with baseline length, but more importantly the visibilities can be seen to vary appreciably with position angle on the sky. This effect is most significant on the longer baselines, indicating that small- rather than large-scale structures are responsible for the deviations from circular symmetry.

These variations with sky position angle could result from a number of complicated brightness distributions, but until much higher angular resolutions can be achieved it seems sensible to restrict attention to a subset of simple models. Of these, at least two can reproduce the modulation in visibility seen at the long baselines: either an overall elliptical distortion of the photosphere or an otherwise circularly symmetric disk on which are superposed a number of compact features displaced from the stellar centre. However, while both of these models predict similar variations in visibility with position angle, they have quite different signatures in the closure phase space, with the elliptical model predicting zero (or 180deg) values always and the “hotspot” model resulting in a complex variation as a function of baseline and baseline orientation.

Our calibrated closure phases for R Cas. are plotted in the lower left panel of Figure 2 for five different closure triangles as a function of position angle on the sky. The systematic variation with position angle is very strong evidence that at least some of the non-circularity of the stellar emission must arise from a non-centrosymmetric structure. The predictions of the model that best fit both the amplitude and phase data — a circular Gaussian with two superimposed bright features (see Table 2 for further details — are plotted in the right hand panels of Figure 2.

Our data analysis thus consisted of fitting sequences of simple models to the visibility amplitude and closure phase data using a conjugate-gradient algorithm to optimise the model parameters. In order to assess the uniqueness of the fits, repeated trials using different initial conditions were made. Here we present fits both for an elliptical Gaussian

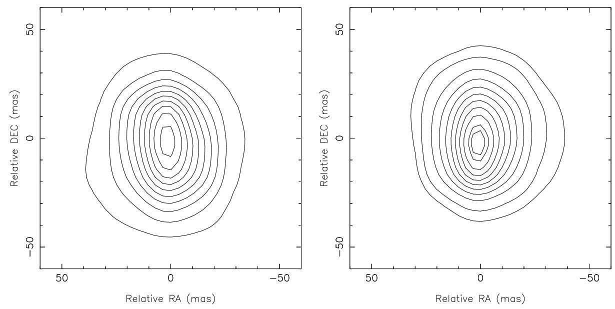

Figure 3. Diffraction-limited image reconstructions of R Cas at 710 nm from data taken in July 1992 (left) and September 1993 (right). The contour levels are plotted from 5% to 95% of the peak flux, at intervals of 10%. North is to the top and East to the left. The map scales are labelled in milliarcseconds.

model, and for models comprising a circular Gaussian with bright asymmetric features. In fitting the latter, models of increasing complexity (with 1, 2, and 3 bright spots) were tried until a satisfactory fit, as measured in a least-squares sense, was obtained. In all instances, models based on Gaussian functions were better fits than those with uniform, hard-edged disks and so we have only included the Gaussian fits here. Further details of our data analysis procedure may be found in (Tuthill et al. 1997).

In a few instances we have confirmed the model-fitting by reconstructing images from the visibility and closure phase data using a Maximum Entropy-based self-calibration algorithm (Sivia 1987). Examples of this are presented in

Table 2. Summary of model-fitting results. For each epoch and wavelength, best-fit details are given for two models: (1) an elliptical disk of Gaussian radial profile and (2) a circular disk of Gaussian radial profile with a number of bright point-like features superimposed. The stellar FWHM and radial co-ordinate of the hotspots (r) are given in milliarcseconds, and θ is measured in degrees North through East. In cases where no hotspot model is listed, the errors on the closure phases were too large to constrain the fitting of asymmetric components. 1-sigma errors are quoted for model parameters.

Object	Date	λ	Elliptical Gaussian			Circular Gaussian		Bright Features			
		nm	fwhm	Ratio	Φ	Flux (%)	fwhm		Flux (%)	r	θ
o Cet	01/92	700	31 ± 1	$.92 \pm .02$	$59° \pm 7°$						
	01/92	710	38 ± 1	$.83 \pm .03$	$58° \pm 6°$						
	07/92	633	28 ± 3	$.80 \pm .12$	$118° \pm 18°$	60 ± 9	36 ± 5	(1)	14 ± 7	15 ± 3	$-57° \pm 12°$
								(2)	17 ± 6	3 ± 1	$+137° \pm 33°$
								(3)	9 ± 4	14 ± 5	$-118° \pm 27°$
	07/92	700	30 ± 2	$.83 \pm .10$	$134° \pm 16°$	66 ± 11	39 ± 5	(1)	16 ± 7	8 ± 6	$-56° \pm 15°$
								(2)	13 ± 6	9 ± 6	$+120° \pm 24°$
								(3)	5 ± 3	16 ± 12	$-157° \pm 32°$
	07/92	710	35 ± 4	$.85 \pm .17$	$119° \pm 20°$	69 ± 12	49 ± 6	(1)	8 ± 5	15 ± 8	$-48° \pm 21°$
								(2)	12 ± 4	3 ± 2	$+94° \pm 30°$
								(3)	11 ± 6	12 ± 7	$-113° \pm 26°$
	01/93	700	29 ± 1	$.87 \pm .02$	$24° \pm 3°$						
	09/93	700	39 ± 1	$.92 \pm .03$	$46° \pm 2°$	95 ± 2	38 ± 2	(1)	5 ± 2	17 ± 2	$+44° \pm 5°$
	09/93	710	49 ± 1	$.96 \pm .02$	$58° \pm 6°$	91 ± 2	54 ± 3	(1)	9 ± 2	11 ± 2	$+59° \pm 8°$
	12/93	700	38 ± 1	$.99 \pm .02$	$38° \pm 19°$	96 ± 3	39 ± 3	(1)	4 ± 3	15 ± 10	$+44° \pm 14°$
	12/93	710	56 ± 1	$.96 \pm .02$	$65° \pm 9°$	87 ± 4	61 ± 4	(1)	13 ± 4	15 ± 3	$+119° \pm 13°$
R Leo	01/92	833	30 ± 3	$.89 \pm .03$	$129° \pm 8°$	87 ± 9	31 ± 3	(1)	13 ± 9	10 ± 5	$+114° \pm 8°$
	06/93	700	40 ± 8	$.96 \pm .25$	$178° \pm 45°$						
	06/93	710	51 ± 5	$.89 \pm .20$	$147° \pm 29°$						
W Hya	06/93	700	48 ± 2	$.93 \pm .08$	$94° \pm 35°$						
	06/93	710	53 ± 2	$.94 \pm .06$	$94° \pm 29°$						
χ Cyg	07/92	700	25 ± 1	$.96 \pm .07$	$102° \pm 42°$						
	06/93	633	25 ± 1	$.89 \pm .02$	$168° \pm 5°$	91 ± 2	23 ± 1	(1)	9 ± 2	14 ± 2	$+168° \pm 4°$
	06/93	700	23 ± 1	$.91 \pm .05$	$160° \pm 15°$	93 ± 7	22 ± 2	(1)	7 ± 7	12 ± 8	$+162° \pm 7°$
	06/93	710	31 ± 1	$.84 \pm .04$	$164° \pm 5°$	92 ± 2	27 ± 1	(1)	8 ± 2	17 ± 3	$+165° \pm 8°$
	09/93	700	30 ± 1	$.89 \pm .04$	$83° \pm 4°$						
R Cas	07/92	700	32 ± 1	$.70 \pm .03$	$7° \pm 9°$	70 ± 10	32 ± 2	(1)	20 ± 5	14 ± 9	$+0° \pm 10°$
								(2)	10 ± 7	8 ± 7	$-151° \pm 11°$
	07/92	710	41 ± 2	$.70 \pm .02$	$1° \pm 7°$	73 ± 5	39 ± 5	(1)	14 ± 3	13 ± 3	$-6° \pm 12°$
								(2)	13 ± 3	9 ± 8	$-163° \pm 7°$
	06/93	700	29 ± 1	$.79 \pm .02$	$20° \pm 5°$						
	09/93	700	29 ± 1	$.80 \pm .01$	$1° \pm 2°$	91 ± 2	24 ± 1	(1)	9 ± 2	21 ± 1	$-177° \pm 3°$
	09/93	710	39 ± 1	$.77 \pm .02$	$2° \pm 3°$	92 ± 5	33 ± 2	(1)	17 ± 5	21 ± 2	$-181° \pm 2°$

Figure 3) which shows image reconstructions of R Cassiopeiae at 710 nm from data secured in 1992 July and 1993 September.

2.3 The sample

The five stars described in this work were drawn from a larger high-resolution imaging survey of 27 evolved giants and supergiants (Tuthill 1994), and were selected on the basis of three criteria; (1) they were long-period variables, (2) they were (comparatively) well resolved, and (3) our imaging experiments yielded high quality complex visibility data. These conditions ensured that only a small subset of the largest and brightest LPV's visible from the WHT were included.

Unfortunately, the quality of the data presented here is not uniform, even for consecutive observations of the same star. There are two main reasons for this. First, the quality of the interferometric data recovered on any given night was strongly dependent upon the seeing conditions on that night, and with only a modest allocation of observing time, it was not possible to obtain data of the highest quality at all times. Second, the targets themselves showed large excursions in magnitude over their variability cycles. This meant that at certain epochs we were obliged to use redundant aperture masks (shaped as slits) to collect sufficient signal. However, this type of mask is less well suited for closure phase measurement (Tuthill 1994), and hence at photometric minimum the Fourier data, especially the phase measurements, were significantly poorer than at maximum.

Table 3. Qualitative morphological descriptions of the sample stars inferred from the detailed model-fits of Table 2. Column 4 gives an estimate of the centro-symmetry of the targets, as assessed by examination of the closure phases, while column 5 denotes the reliability of our knowledge of the source structure based on the signal-to-noise and internal consistency of the data.

Object	Epoch	Morphology	Symmetry	Confidence
o Cet	Jan 92	Elongation at 60°	Unknown	High
	Jul 92	Disk + $\sim$ 3 spots	Asymmetric	Fair
	Jan 93	Elongation at 25°	Unknown	Low
	Sep 93	Disk + 1 spot at 50°	Asymmetric	High
	Dec 93	Disk + 1 spot at 120°	Asymmetric	Fair
R Leo	Jan 92	Disk + 1 spot at 115°	Asymmetric	High
	Jun 93	Elongation at $0 \sim -30°$	Unknown	Low
W Hya	Jun 93	Elongation, PA 100°	Unknown	Fair
χ Cyg	Jul 92	Elongation at 5°	Unknown	Low
	Jun 93	Disk + 1 spot at 160°	Asymmetric	High
	Sep 93	Elongation at 80°	Unknown	Low
R Cas	Jul 92	Disk + 2 spots	Asymmetric	High
	Jun 93	Elongation at 20°	Unknown	High
	Sep 93	Disk + 1 spot at 180°	Asymmetric	High

3 RESULTS

Our results are summarised in Table 2. This gives the parameters of the best-fitting models for each star at each colour and epoch of observation. Where the data quality is good enough, results for both the elliptical Gaussian and "hotspot" model have been given. For the lower signal-to-noise data, although it was always possible to fit the data with a "hotspot" model, its parameters were often very poorly constrained, and so in these cases we have only listed the parameters of the elliptical Gaussian fit. The absence of a bright spot model in Table 2 thus simply indicates poorer data quality and in no way favours the elliptical model.

3.1 The nature of asymmetries

The most obvious conclusion to be drawn from Table 2 is that deviations from circular symmetry appear to be ubiquitous amongst the sample. In those cases when high quality closure phases were measured the stars invariably showed the signatures of non-centrosymmetric structure, and where multi-colour observations were made at the same epoch the resulting best-fit model parameters generally showed broad agreement.

A condensed summary of the morphologies implied by Table 2 is presented in Table 3. This is intended to give a qualitative precis of the contents of Table 2 together with an estimate of the confidence, based upon the data quality and internal consistency, that the morphological classification is a reliable description of the true stellar flux distribution. An interesting feature of Table 3 is that at no time were high-quality closure phases of zero (or 180°) measured for any of the targets, whereas in general all the unresolved calibrator stars gave closure phases of 0°. It seems plausible to speculate, therefore, that, at least for these long period variables, all the departures from circular symmetry may have arisen from non-centrosymmetric distortions, but that these were not always detected directly due to limitations in the signal-to-noise of our measurements. This mirrors the situation in the literature, where authors with little or no phase information tend to model their high resolution data in terms of elliptical structures (Karovska et al. 1991; Wilson et al. 1992; Quirrenbach et al. 1992; Lattanzi et al.1997) while those with phase information often prefer interpretations based on asymmetric features (Weigelt et al. 1996; Tuthill et al. 1997; Bedding et al. 1994; Burns et al. 1998).

3.1.1 Evolution timescale

It is apparent from Tables 2 and 3 that the individual stellar morphologies can change markedly from one epoch to the next. An example of this is shown in Figures 4 and 5. These display the visibility amplitudes and closure phases measured for *o* Ceti in 1992 July and 1993 September (the intervening observation in January 1993 was of low quality as the star was near minimum light).

In 1992 the relatively complex behaviour of the data, particularly the closure phases, required the most complicated model encountered in order to produce an adequate fit. The predicted Fourier data for this Gaussian disk + three spot model (see Table 2) are plotted in the right-hand panels of Figure 4. They reproduce the observed variations well, with the exception of some of the excursions at high visibility. In this regime calibration of the visibility amplitude is often difficult, and this may be the reason for the unmodelled variation seen on the very shortest baselines. For comparison Figure 5 shows the equivalent data taken just over one year later. The form of the visibility and closure phase modulation is markedly different, and can be fit very well with a simpler model consisting of a Gaussian disk with a single bright asymmetric spot.

Such changes in the stellar emission were not always encountered, and in certain instances particular features could

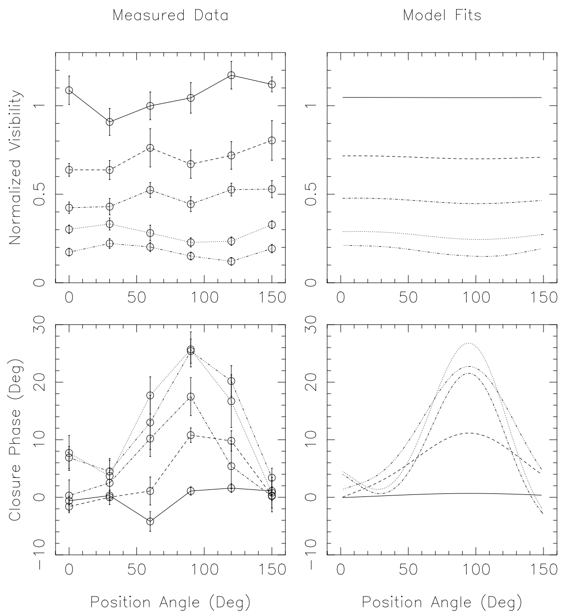

Figure 4. Calibrated visibility amplitudes and closure phases for *o* Ceti at 710 nm measured 1992 July. The left-hand panels show the measured data, and the right-hand panels the fits for a model composed of a Gaussian disk with three unresolved bright spots on the stellar surface.

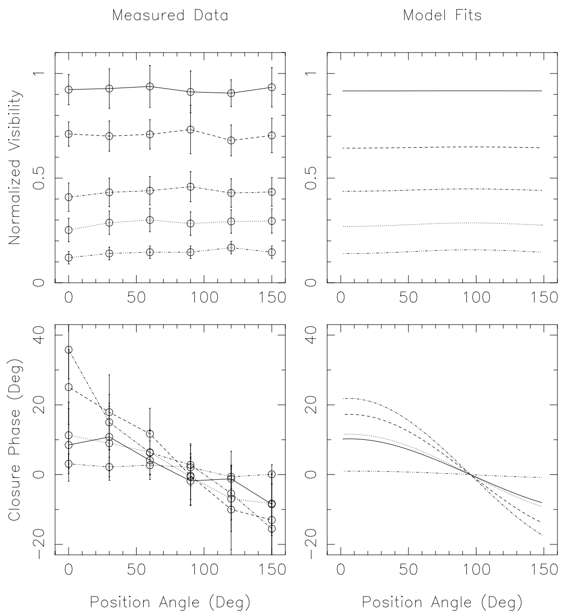

Figure 5. Calibrated visibility amplitudes and closure phases for o Ceti at 710 nm measured in 1993 September. As before, the left-hand panels show the measured data, and the right-hand panels the fits for the model – in this case a Gaussian disk with one unresolved feature on the stellar surface.

be traced for many months. This can be seen in the case of *o* Ceti by comparing its emission observed in 1993 December, some 90 days following the 1993 September data discussed above. If the Gaussian + Bright Spot models for these two epochs are compared, then at 700 nm they appear almost identical, with a feature contributing about 5% of the stellar flux persisting at a radius of ∼15 mas and P.A. of 44° from the centre of the star.

Although the equivalent fits at 710 nm are similar in most regards, there appears to be a significant rotation in the location of the hotspot between the two observations. Since the 700 nm filter used samples continuum radiation, while the 710 nm filter isolates a strong TiO bandhead (implying that we are looking at the higher, cooler regions of the stellar atmosphere) the inconsistency between the 710 nm measurements may simply be due to changes in the tenuous outer layers of the star. This is consistent with the earlier study of Tuthill, Haniff & Baldwin. (1995) who showed that the molecular atmosphere of *o* Ceti was greatly distended during this period, most noticeably in the 710 nm TiO band, due to the passage of an aperiodic shock through the stellar atmosphere.

Secular changes in the shape of *o* Ceti have been the subject of a variety of studies with Karovska el al. (1991) and Quirrenbach el al. (1992) finding a variable position angle and axial ratio for elliptical models, while Wilson et al. (1992) argued for a constant distortion over some four pulsational periods. The data presented here suggest that changes in the appearance of *o* Ceti arise from the evolution of bright features, rather than gross distortions of the overall stellar atmosphere and, if our results are representative, occur on timescales of between 3 and 14 months.

The other star for which high quality data were secured at successive epochs was R Cas. In this case a gross elongation at a position angle of ∼ 0° persisted in the stellar images from 1992 July through to 1993 September. The distortion was seen to weaken somewhat with time, with the axial ratio of the best-fit ellipse changing from an initial value of approximately 0.7 in 1992 July to 0.8 in June and September of the following year. As for the other stars in this study, the elongations were found, on the basis of the measured closure phases, to contain a strong asymmetric component. An examination of the results in Table 2 shows that the longevity of the "elongation" was in fact due to the persistence of a single bright feature, located in the southern hemisphere of the stellar disk. However, while this feature was relatively long-lived, a bright feature towards the north of the star was seen to fade, resulting in a decrease in the apparent "ellipticity" of the star.

R Cas. was also observed at high resolution with the Russian 6 m SAO telescope one year after our last measurement (Weigelt et al. 1996). Fortunately the observing wavelengths and resolutions obtained by these authors were similar to those reported here, and allow a direct comparison of their data and ours. If we first consider their elliptical model fits, Weigelt et al. report axial ratios of 0.86 and 0.75 at position angles of 52° and 57° for observations at 700 and 715 nm respectively. Thus, although the magnitude of the axial ratios are in general agreement with our measurements, the angle of the major axis appears to have rotated significantly over a timescale of a year. Interestingly, (Weigelt et al. 1996) also obtained much better fits to their data using models consisting of a circular disk with 2 bright asymmetric features. Although the locations of their features bears no resemblance to the fits presented in Table 2, it is reassuring to note that the broad features of their models, e.g. the number of spots (2) and their fractional fluxes (14% and 11%), are remarkably consistent with ours. Our observations, together with those of (Weigelt et al. 1996) thus support a picture where bright features on the surface of R Cas. evolve on timescales of about one year.

3.2 Model parameters

Before discussing our results, we caution the reader against taking the model parameters from Table 2 as *precise* representations of the stellar brightness distribution. Although care was taken to ensure that models with the smallest number of free parameters were always used to characterise our data, it was *not* the case that all aspects of the models were always well constrained.

In particular, the lack of measurements on baselines longer than 4 m meant that we were often unable to explore the visibility function beyond its first null. In this case a particular dataset might have been equally well fit by a model with a bright spot at a small radius from the centre of a circular stellar disk, or by a model with a fainter spot located at a larger radius. These problems were greatly exacerbated for more complex models with two or three bright spots, and generally highlight the need for measurements on longer baselines that can only be provided by the latest 10 m class telescopes or separated-element interferometers.

Model fitting was also attempted using dark, rather than bright features superposed on the stellar disk. Although we found that dark spot models could produce adequate fits, many more degrees of freedom were required than for the corresponding bright-spot model. Thus although we cannot rule out the possibility of dark spots existing on these stars, because these models were always more contrived, we hereafter will only discuss the bright spot models.

3.3 Discussion

In the past, a number of different mechanisms have been proposed to explain the departures from circularity seen in Mira variables including stellar rotation, interaction with a companion, and patchy circumstellar extinction/scattering. However, the characteristic timescales expected for these phenomena are much longer than the yearly evolution time observed for the features reported here. Models invoking non-radial pulsation might be consistent with such a shorter timescale, but it is not yet clear whether these would be observed directly as distortions in the stellar photosphere.

Given that our data have highlighted the existence of localised regions of brighter emission, two plausible mechanisms present themselves. The first of these has already been elaborated for supergiant stars as the origin of the "hotspots" seen in interferometric images of their surfaces (see, e.g. Tuthill et al. 1997) and identifies these features with the tops of very large convection cells. The observational properties of the features reported here are very similar to those seen in M supergiants, and could be explained in terms of a small number of bright zones each covering ~10% of the stellar disk and with a temperature excess of a few hundred Kelvin.

An alternative idea, recently proposed to explain the asymmetries seen on the surface of α Orionis is that these are associated with shock waves induced by pulsations of the stellar envelope (Uitenbroek, Dupree, & Gilliland 1998). While this model appears well suited to Mira variables, where both theoretical models and optical spectra show clear evidence for the formation of pulsation-induced shocks in their tenuous atmospheres, it is less clear whether these can generate the compact structures suggested by our measurements.

If either these models is correct, a remaining problem will be to relate the asymmetries close to the stellar surface to those seen in the dust shells surrounding many late type systems. The adaptive optics data of Cruzalèbes et al. (1998) suggest an extremely clumpy distribution of dust within $1''$ of o Ceti, though how these might be associated with deeper asymmetries remains unclear.

4 CONCLUSIONS

We have used interferometric methods to image the surfaces of five Mira variables in the optical/near-infrared. All of the sample stars exhibited strong departures from rotational symmetry, and in those cases where Fourier phase information was obtained with high signal-to-noise the best-fit models were generally non-reflection symmetric. The stellar surfaces were seen to change over time, with characteristic timescales ranging from several months to a year. Our observations suggest some form of transient surface activity, which we tentatively identify with either convective upwellings or the passage of localised shocks through the stellar atmosphere. Theoretical efforts in modelling convection, in addition to higher angular resolution data will be required to identify the origin of these phenomena uniquely.

ACKNOWLEDGMENTS

Financial support from the Royal Society (CAH), the Cambridge Commonwealth Trust and the Cambridge Philosophical Society (PGT) are gratefully acknowledged. We are also grateful to the many members of our group, without whom the observations reported here would not have been possible. The Caltech VLBI package written by Tim Pearson with modifications from Joseph Lehar has been used in producing maps and fitting models for this work. The William Herschel Telescope is operated on the island of La Palma by the Royal Greenwich Observatory in the Spanish Observatorio del Roque de los Muchachos of the Instituto de Astrofísica de Canarias.

REFERENCES

Bedding, T.R., Zijlstra A.A., von der Luhe O., Robertson, J.G., Marson, R.G., Barton J.R., Carter B.S., 1994, AA, 290, 240

Burns D., Baldwin J.E., Boysen R.C., Haniff C.A., Lawson P.R., Mackay C.D., Rogers J., Scott T.R., St-Jacques D., Warner P.J., Wilson D.M.A., Young J.S., 1998, MNRAS, 297, 462

Buscher D.F., Haniff C.A., Baldwin J.E., Warner P.J., 1990, MNRAS, 245, 7p

Cruzalèbes, P., Lopez, B., Bester, M., Gendron, E., Sams, B., 1998 AA, 338, 132

Gilliland R.L. Dupree A.K., 1996, ApJ, 463, L29

Haniff, C.A., Mackay, C.D., Titterington, D.J., Sivia, D., Baldwin J.E., Warner P.J., 1987, Nat, 328, 694
Haniff, C.A., Buscher, D.F., 1992, JOSA, A, 9, 203
Haniff C.A., Scholz M., Tuthill P.G., 1995, MNRAS, 276, 640
Karovska M., Nisenson P., Papaliolios C., Boyle R.P., 1991, ApJ, 374, L51
Kholopov P.N., 1987, General Catalogue of Variable Stars, Fourth Edition. Nakua Publ. House, Moscow
Lattanzi M.G., Munari U., Whitelock P.A., Feast M.W., 1997, ApJ, 485, 328
Lim J., Carilli C.L., White S.M., Beasley A.J., Marson R.G., Haniff C.A., Mackay C.D., Titterington D.J., Sivia D., 1998, Nat, 392, 575
Quirrenbach A., Mozurkewich D., Armstrong J.T., Johnston K.J., Colavita M.M., Shao M., 1992, A&A, 259, L19
Sivia D.S., 1987, Ph.D. Thesis, University of Cambridge
Tuthill P.G., 1994, Ph.D. Thesis, University of Cambridge
Tuthill P.G., Haniff C.A., Baldwin J.E., Feast M.W., 1994a, MNRAS, 266, 745
Tuthill P.G., Haniff C.A., Baldwin J.E., 1994b, in Robertson J.G., Tango W.J., eds, Proc. IAU Symp. 158, Very High Angular Resolution Imaging. Kluwer, Dordrecht, p. 395
Tuthill P.G., Haniff C.A., & Baldwin J.E. 1995, MNRAS, 277, 1541
Tuthill P.G., Haniff C.A., & Baldwin J.E. 1997, MNRAS, 285, 529
Uitenbroek, H., Dupree, A.K. & Gilliland, R.L., ApJ, In press
Weigelt G., Balega Y., Hofmann K.-H., Scholz M., 1996, AA, 316, L21
Wilson R.W., Baldwin J.E., Buscher D.F., Warner P.J., 1992, MNRAS, 257, 369

APPENDIX A: STELLAR DIAMETERS

The 5 stars featured in this paper were taken from a larger programme of diffraction-limited imaging which targeted 27 evolved giants and supergiants, full details of which can be found in Tuthill (1994a). Much of the data taken in this study has been published in papers on the atmospheres of Miras (Tuthill, Haniff & Baldwin 1994b; Haniff, et al. 1995; Tuthill et al. 1995) and red supergiants (Tuthill et al. 1997). However, there were some 14 stars for which the data quality was not sufficiently high, and which were not sufficiently well resolved to be included in these previous studies. We include measurements of these stars in Table A1 as a reference for other workers in the field.

This paper has been produced using the Blackwell Scientific publications LaTeX style file.

Table A1. Observing log and best-fitting one-parameter models for the remainder of the sample stars. Below the star name in column 1 is the (Kholopov 1987) designation of its variability type where 'M' denotes a Mira-type variable and 'SRb' denotes a class of semi-regular variable. The variability of two further stars, CH Cyg and R Aqr is complicated by the presence of a close companion and they have been designated symbiotic (Symb.). Mira periods are from Kholopov (1987) and pulsation phases have been determined from AAVSO records (Mattei, private communication). Filter wavelengths are measured in nm. The timings of the observations are identified by the calendar date of the night of the observation. For the uniform-disc (UD) fits the diameter is given, whereas for Gaussian models the full width at half maximum is quoted. 1σ errors are shown.

Object & period (d)	Date (d/m/y)	Stellar phase	Filter $\lambda/\Delta\lambda$	UD (mas)	Gaussian (mas)
SS Vir	03/01/93	0.06	833/41	19.5 ± 2.0	11.6 ± 1.2
M 355					
V CVn	13/07/92	0.15	833/41	24.2 ± 3.0	14.6 ± 2.0
M 192	02/01/93	0.10	700/10	29.4 ± 2.5	17.8 ± 1.6
R CVn	13/07/92	0.06	833/41	$\lesssim 24$	$\lesssim 14$
M 328					
S CrB	13/07/92	0.19	833/41	21.7 ± 3.0	13.0 ± 1.8
M 361					
V CrB	13/07/92	0.12	833/41	21.1 ± 2.0	12.9 ± 1.2
M 358					
R Ser	13/07/92	0.27	700/10	16.0 ± 7.0	10.0 ± 4.0 P
M 357	13/07/92	0.27	833/41	15.0 ± 5.0	9.0 ± 3.0 P
U Her	09/06/93	0.02	700/10	33.6 ± 6.0	20.3 ± 3.6 P
M 406	09/06/93	0.02	710/10	35.4 ± 4.0	20.6 ± 2.5 P
	07/06/93	0.02	902/50	19.9 ± 3.0	11.9 ± 2.0
30 Her	11/07/92	–	700/10	$\lesssim 20$	$\lesssim 12$
SRb	11/07/92	–	710/10	20.0 ± 3.0	12.1 ± 1.8
X Oph	13/07/92	0.27	833/41	21.8 ± 6.0	13.0 ± 4.0 P
M 334					
R Lyr	12/07/92	–	710/10	$\lesssim 20$	$\lesssim 12$
SRb					
CH Cyg	07/06/93	–	700/10	20.0 ± 4.0	10.8 ± 2.5 P
Symb.	09/06/93	–	710/10	24.2 ± 2.8	15.2 ± 1.8
R Cyg	12/07/92	0.16	833/41	$\lesssim 24$	$\lesssim 14$
M 426					
R Aqr	13/07/92	–	830/41	23.4 ± 4.0	14.3 ± 2.5 P
Symb.					